

The stellar host in blue compact dwarf galaxies: the need for a two-dimensional fit

Ricardo O. Amorín¹, Casiana Muñoz-Tuñón¹, J. Alfonso L. Aguerri¹, Luz M. Cairós²
and Nicola Caon¹

¹ Instituto de Astrofísica de Canarias (IAC), Vía Láctea, E-38200 La Laguna, Tenerife, Spain

e-mail: ricardo.amorin@iac.es, casiana@iac.es, jalfonso@iac.es nicola.caon@iac.es

² Astrophysikalisches Institut Potsdam, An der Sternwarte 16, D-14482 Potsdam, Germany

e-mail: luzma@aip.de

Received, 2006 August 1; accepted 2007 February 12

ABSTRACT

Context. The structural properties of the low surface brightness stellar host in blue compact dwarf galaxies are often studied by fitting $r^{1/n}$ models to the outer regions of their radial profiles. The limitations imposed by the presence of a large starburst emission overlapping the underlying component makes this kind of analysis a difficult task.

Aims. We propose a two-dimensional fitting methodology in order to improve the extraction of the structural parameters of the LSB host. We discuss its advantages and weaknesses by using a set of simulated galaxies and compare the results for a sample of eight objects with those already obtained using a one-dimensional technique.

Methods. We fit a PSF convolved Sérsic model to synthetic galaxies, and to real galaxy images in the B , V , R filters. We restrict the fit to the stellar host by masking out the starburst region and take special care to minimize the sky-subtraction uncertainties. In order to test the robustness and flexibility of the method, we carry out a set of fits with synthetic galaxies. Furthermore consistency checks are performed to assess the reliability and accuracy of the derived structural parameters.

Results. The more accurate isolation of the starburst emission is the most important advantage and strength of the method. Thus, we fit the host galaxy in a range of surface brightness and in a portion of area larger than in previous published 1D fits with the same dataset. We obtain robust fits for all the sample galaxies, all of which, except one, show Sérsic indices n very close to 1, with good agreement in the three bands. These findings suggest that the stellar hosts in BCDs have near-exponential profiles, a result that will help us to understand the mechanisms that form and shape BCD galaxies, and how they relate to the other dwarf galaxy classes.

Key words. galaxies: dwarf – galaxies: evolution – galaxies: photometry – galaxies: starburst – galaxies: structure

1. Introduction

Blue compact dwarf (BCD) galaxies have been recognized for some time as playing an important role in our understanding of star formation (SF) processes, and their study provides relevant information for our knowledge of the evolution of galaxies. BCDs are gas-rich (H I mass fraction typically higher than 30%) and metal-deficient ($Z_{\odot}/50 \leq Z \leq Z_{\odot}/2$) extragalactic systems, which display very intense and narrow emission lines in the optical (similar to those seen in H II regions), due to the intense SF activity distributed in one to several star-forming bursts (Cairós et al. 2001b, hereafter C01b). Stars are formed at high rates ($0.1\text{--}1M_{\odot}$, Fanelli et al. 1988), exhausting their gas content in much shorter times than the age of the Universe. The mechanisms triggering the cloud collapse in

these low mass systems is still unknown since, unlike in normal spirals, density waves are inhibited. Moreover, their characteristics are believed to have been common among unevolved low-mass galaxies at high to intermediate redshift. Local BCDs are therefore the most suitable nearby laboratories for studying the spectrophotometric and chemodynamic properties of distant and faint galaxies counterparts at high spatial resolution.

The nature and genesis of BCDs have been studied and are now better understood. The idea of BCDs being genuinely young galaxies forming stars for the very first time (Sargent & Searle 1970; Kunth et al. 1988) is now discarded, at least for the vast majority of them. Deep photometric studies in the optical (Loose & Thuan 1986; Telles 1995; Papaderos et al. 1996b; Doublier et al. 1997,1999; Cairós 2000; Cairós et al. 2001a, hereafter C01a; C01b; Bergvall & Östlin 2002) and in the near-infrared (Noeske et al. 2005, and reference therein) have in fact

revealed that virtually all BCDs present a low-surface brightness (LSB) stellar host. This stellar component, underlying the SF regions, is an extended envelope that generally shows elliptical isophotes, displays red colours, indicative of an evolved stellar population (Papaderos et al. 1996b; C01a; C01b; Cairós et al. 2002; Cairós et al. 2003; Bergvall & Östlin 2002), and is therefore a “witness” of former events of star formation.

LSB hosts are typically found to dominate the intensity and colour distribution of BCDs for $\mu_B \gtrsim 24$ mag/arcsec⁻² (Papaderos et al. 1996b; C01b). This evolved stellar population is observed in all types of BCDs, except for the extremely rare i0 type (from the classification scheme of Loose & Thuan 1986).

In order to establish the luminosities, structures and evolutionary status, as well as the star-forming history of BCD galaxies, it is indispensable to characterize the LSB component underlying the starburst regions. The first step in this process is to derive the LSB host ages and chemical abundances. Also, a comprehensive spectrophotometric study of the starburst in BCDs needs a precise determination of the structural properties of the LSB stellar host in order to remove its contribution. Moreover, the structural, kinematic and dynamical properties of the host galaxy in BCDs are important issues in dwarf galaxy research, as they help to understand such processes as the regulation of the SF activity, and the possible evolutionary connections between different dwarf galaxy types.

Vaduvescu et al. (2006) show, from *NIR* surface photometry, that the starburst is usually a small fraction of the total mass. Furthermore, provided that dark matter does not dominate the mass within the Holmberg radius (Papaderos et al. 1996b), the LSB component is, together with the H I halo, mainly responsible for the global gravitational potential within which the starburst phenomenon takes place. Thus, the analysis of the projected luminosity distribution is fundamental for modelling the gravitational potential and the dynamics of BCDs, as well as the effects of starburst events in their interstellar medium, such as galactic winds. Whether the processed stellar material will be released, causing the contamination of the intergalactic medium, depends strongly on the galaxy structure (Tenorio-Tagle et al. 2003), being easier in disc-like objects than in spheroids (Silich & Tenorio-Tagle 2001, see their Fig.3).

The comparison of the properties of the LSB stellar component (e.g. structural parameters, average colours, and colour gradients) with those of other dwarf galaxy classes (dwarf irregulars, dIs; dwarf elliptical, dEs), and low-surface brightness galaxies is crucial for testing those evolutionary scenarios that link these galaxies with BCDs (Thuan 1985; Davies & Phillipps 1988; Papaderos et al. 1996a; Marlowe et al. 1997, 1999; Cairós 2000).

The faint surface brightness of the LSB component and the contamination caused by the starburst emission make the derivation of the structural parameters of the underlying host in BCDs a complicated task. Thus, the derived structural parameters strongly depend on how well the starburst has been excluded from the fit, on the extent of the fitted LSB radial profile, on the quality of the dataset, and on the method and model used to parameterize the surface brightness profile.

Some previous studies, in which one-dimensional models of the BCDs LSB component were fitted, have shown discrepant results even for the same galaxies, especially when a Sérsic law was applied (see examples in Cairós et al. 2003 and Caon et al. 2005). Moreover, during the extraction of a radial profile one can find serious limitations and ambiguities. Each of the different procedures has its own drawbacks, resulting in information loss from the image (Baggett et al. 1998).

At the present time, several well-tested two-dimensional algorithms are available. There are also several examples in the literature of studies showing that the two-dimensional method is generally more reliable than one-dimensional methods in bulge–disc decompositions (de Jong 1996), as it is able to retrieve more accurate structural parameters. Particularly in BCDs, a two-dimensional fit to the image, by using a χ^2 minimization technique, may provide significant advantages over the fit to some averaged one-dimensional profile.

In Caon et al. 2005 (hereafter Paper I) we presented a very detailed one-dimensional Sérsic fitting of a sample of eight BCDs, showing that by carefully selecting the fitted radial range and by performing consistency checks on the fits we can derive reliable structural parameters. We also analysed in detail the problems and uncertainties involved in the fitting of a 1D Sérsic model.

As a natural continuation of the work in Paper I, here we explore the LSB stellar host structural characterization by carrying out a two-dimensional fitting technique to the same galaxies. We propose a consistent methodology, explain its advantages and discuss its possible drawbacks and limitations.

One of the crucial issues to be investigated is whether or not there is an evolutionary link among the different classes of the dwarf galaxies population. Although detailed studies of individual objects are important and can provide tests, examples, or counterexamples, which are undoubtedly useful, statistical studies are the key for extending or establishing general paths. To do so, “semiautomatic” procedures able to analyse a large data base are necessary. In particular, to classify the LSB host into structures with low or high n Sérsic index with well-controlled uncertainties would be an important first step. In Section 2 we present the sample of galaxies; in Section 3 we describe the two-dimensional fitting methodology. Simulations with synthetic galaxies are described in Section 4. In Section 5 we discuss the observational uncertainties involving the fitting of a Sérsic model to the BCDs host galaxy. Section 6 presents the results of the 2D fitting to the sample of galaxies. Summary and conclusions are the subject of Section 7.

2. The Sample

Eight galaxies were selected from a larger sample of 28 BCDs already studied by our group. A complete description of this sample, as well as the image reduction and calibration procedures, were given in C01a and C01b. The complete collection of broad-band and H α images of the galaxies can be found online ¹.

¹ see <http://www.iac.es/proyect/GEFE/BCDs/BCDframe.html>

We have selected the same objects already analysed in Paper I. Such galaxies are those with the deepest images, located in areas of the sky free from nearby bright stars, and with few overlapping background or foreground objects. The basic data on the galaxies are presented in Table 1.

3. The Two-Dimensional Fitting Method

It is clear that many BCDs present light profiles with significant deviations from a pure exponential (Cairós et al. 2003; Paper I). Following our previous works (Cairós 2000, C01a, Cairós et al. 2003, and Paper I) we have adopted the Sérsic law (Sérsic 1968) to fit our data. This paper does not concern itself with which mathematical function best suits the surface brightness profiles of most BCDs host galaxies. The applicability of the Sérsic profile and the drawbacks associated with it were the subject of Paper I. This profile has been shown to describe the light distribution in ellipticals (from dwarfs to brightest cluster members, Caon et al. 1993, Young & Currie 1994, Graham et al. 1996, Graham & Guzmán 2003, Aguerri et al. 2005) and spiral bulges (Prieto et al. 2001). Here, for the first time, a new methodology for fitting BCD hosts by using a two-dimensional technique is developed. We used the publicly available software called GALFIT v2.0.3b (Peng et al. 2002; hereafter P02). Detailed information on GALFIT and how it is implemented can be found in P02, and on-line.² GALFIT has been used in recent years in several works where modelling of the light distribution of galaxies was required, e.g. in disc galaxies (Barden et al. 2005), field spheroidal and bulge-dominated galaxies (Treu et al. 2005), active galaxies (Sánchez et al. 2004; Dong & De Robertis 2006) and luminous blue compact galaxies (Noeske et al. 2006), among others. However, it has not yet been applied to blue compact and irregular dwarfs. We give here a brief introduction on how GALFIT works and describe the methodology we implemented and applied to fit our galaxies. GALFIT was designed to extract structural components from galaxy images, as it is capable of fitting a galaxy with an arbitrary number of components simultaneously, whose geometry is described by axially symmetric generalized ellipses (see Athanassoula et al. 1990), and whose profile can be one of several analytic functions such as Sérsic, Gaussian, exponential, or a constant or tilted background. The program has the option of convolving the models with the point-spread function (PSF) to simulate the seeing. GALFIT minimizes the χ^2_v (normalized χ^2 , see P02) residuals using a downhill gradient/parabolic expansion method, called Levenberg-Marquardt (Press et al. 1997), by iteratively creating model images, convolving them with the PSF and subtracting them from the data. Also, GALFIT is able to use the readout noise and gain parameters of the image to build a Poissonian noise model in order to weigh the pixels used in the fit. In our case, we fitted a single Sérsic model:

$$I(r) = I_e e^{-b_n [(r/r_e)^{1/n} - 1]}, \quad (1)$$

where I_e is the intensity at the effective radius r_e that encloses half of the total light from the model (Caon et al. 1993), while the constant b_n is coupled with the Sérsic shape parameter, n . The generalized ellipses:

$$r = \left(|x - x_c|^{2+c} + \left| \frac{y - y_c}{q} \right|^{2+c} \right)^{1/(2+c)} \quad (2)$$

can be rotated to any position angle (PA). The parameter q is the axis ratio of the model. The parameter c is positive for boxy isophotes, and negative for discy ones.

The flux, integrated over all radii for an elliptical Sérsic profile with an axis ratio q , is given (following the notation by P02) by:

$$F_{tot} = 2\pi r_e^2 \Sigma_e e^{k_n} n k_n^{-2n} \Gamma(2n) q / R(c), \quad (3)$$

where $\Gamma(2n)$ is the Gamma function, and

$$R(c) = \frac{\pi(c+2)}{4\beta(1/(c+2), 1+1/(c+2))}, \quad (4)$$

where $\beta(1/(c+2), 1+1/(c+2))$ is the beta function with two arguments. $R(c)$ is a function that accounts for the area ratio between a perfect ellipse and a generalized ellipse of discyness/boxyness parameter c (P02).

In total, we have 8 free parameters: x_c , y_c , m_{tot} , r_e , n , q , PA , and c . Note that the same number of parameters must be determined in a one-dimensional Sérsic fit.

3.1. Implementation

We prepare the images (galaxy and PSF) and the GALFIT input files. Here we select the appropriate model we want to fit. Then, we identify the starburst emission from the image and make a set of elliptical (preliminary) masks in order to mask-out that emission from the fit. Next, we perform a set of fits and plot the output parameters versus the size of the masks. From that and the residual images we identify both the range of mask sizes where the parameters fit data with the minimum scatter, and the mask outside which the starburst emission is practically absent. Afterwards, we use the residual image to refine the size and shape of the mask and we fit again with the new mask in an iterative process. Finally, the procedure stops when the best solution is obtained. A sketch of the procedure is shown in Fig.2. The method is described in detail as follows:

1 - Preparing the images and the input files

Reduced and calibrated images were cleaned for bad pixels, cosmic ray events, and other artefacts. In some cases, the edge of the images were trimmed (Paper I) in order to eliminate spurious sources and vignetting. Background and foreground objects were masked out by using *DS9* and the IRAF/PROS task *plcreate*. Images were corrected (Paper I) for small large-scale variations in the sky background by fitting and subtracting out a low-order polynomial, using the IRAF task *imsubfit*.

GALFIT requires a first-guess set of parameters to be given in an input file. We used the same m_{tot} , r_e , n values published in Paper I; for x_c , y_c , PA q we used mean values averaged outside the starburst region from the isophote fitting carried out in Paper I, while c was set to 0.

² <http://zwicky.as.arizona.edu/cyp/work/galfit/galfit.html>

Finally, GALFIT allows us to optionally fit also the sky-background as a plane that can tilt in x and y :

$$sky(x, y) = sky(x_0, y_0) + (x - x_0) \frac{dsky}{dx} + (y - y_0) \frac{dsky}{dy} \quad (5)$$

We discuss the application of this option in § 4.

2 - The input PSF

As we already mentioned, GALFIT uses a PSF image in order to simulate the seeing and convolve it with models. When fitting the central pixels of a light distribution, the convolution can be very important since the effects of seeing are more significant (Trujillo et al. 2001a,b). Since it is the most accurate way to do it, we extracted a PSF image directly from the data, finding an unsaturated star with high S/N .

3 - Elaboration of input masks

When fitting the radial surface profiles of the LSB component in BCDs, the determination of the radial interval is critical (Paper I). Whatever the technique employed, we must make sure that we fit only those regions free from the starburst (young stars+gas). So, when fitting an image, we need to mask out the area of the galaxy occupied by the starburst, whose identification is not always straightforward.

Colour maps and $H\alpha$ images (when available) could help to identify and delimit the starburst emission, and thus define a “first order” size and shape of the masks. However, a more accurate determination of the region where the starburst is practically absent is needed when fitting a Sérsic function. In order to do this, an iterative procedure described below, has been applied. The input masks for fitting consist of a set of elliptical masks of different sizes. We have used the IRAF tasks *plcreate* and *imreplace* in order to create masks of the same size as the input image, with value 0 in those regions to be fitted (“starburst-free region”) and value 1 in the region we want to mask out from the fit (“starburst region”). The size of these masks go from the small ones containing the inner isophotes, i.e. masking out the starburst peak(s), up to the larger ones, following the shape of the outer isophotes, ensuring that we mask out the entire starburst emission.

4 - Searching for Stability

The derived parameters may strongly depend on the masked area of the galaxy. Small masks that do not contain all of the starburst emission or very large masks extending far into the starburst-free region are both expected to produce unreliable and/or large uncertainties in the fitted parameters. In Paper I we used two variables: the transition radius, R_{tran} as the radius beyond which starburst emission is absent, and R_{max} , the outermost point fitted. The quantity $R_{\text{max}} - R_{\text{tran}}$ then indicates the fitted radial interval where the fit is stable, i.e. the parameters fits with the minimum scatter.

Successive fits with elliptical input masks of different sizes is a possible way of estimating both R_{tran} and the stability of a given parameter, as the range of the light distribution that gives the minimum scatter. Since GALFIT fits the entire image, weighting each pixel with its own noise, we cannot set an outer

radius (i.e. R_{max}) for the fit, so it is difficult to estimate $R_{\text{max}} - R_{\text{tran}}$.

Instead, we prefer to quantify the percentage of galaxy pixels we actually mask out from fit, P_{area} , defined as

$$P_{\text{area}} = 100 \left(\frac{N_{\text{mask}}}{N_{\text{gal}}} \right) = 100 \left(\frac{R_{\text{mask}}}{R_{\text{gal}}} \right)^2, \quad (6)$$

where N_{mask} is the number of pixels masked out, contained in a circle of radius R_{mask} , and N_{gal} is the total number of pixels with $S/N > 1$, contained in a circle of radius R_{gal} . The quantity $100 - P_{\text{area}}$, when $R_{\text{mask}} = R_{\text{tran}}$, quantifies the fraction of the galaxy (with $S/N > 1$) free of starburst emission we actually fit.

In the fitting procedure, we progressively increase the mask size, starting from a mask somewhat smaller than the starburst and ending with a mask significantly larger than the starburst. In this way, we aim to detect sudden changes in the structural parameters, which could indicate a significant contamination by the starburst light, i.e. a rough estimation of the transition radius.

The number of masks, and thus of independent fits, varies depending upon the galaxy size, but between six and ten is usually enough to generate a “stability plot” in which the structural parameters are represented versus P_{area} (and/or R_{mask} , see Figs. 4-6). The step between masks, i.e. the step in R_{mask} , depends on the extension of the starburst in each filter for a given galaxy. Each fit with a given mask is carried out twice with a fixed sky value and a sky value free to vary in the fit. As we shall discuss later, the difference between the values for the Sérsic parameters in the two cases gives us a further estimation of the uncertainties on fitting the LSB component. The procedure can be automatized up to this point.

5 - The Final Mask

From the stability plots we identify the best model, i.e. the one in which the starburst has been completely masked out (see asterisks in Figs. 4-6). From that model we determine the P_{area} range where the parameters do not change significantly (e.g. see grey band in Fig. 8). We inspect the residual images (galaxy – model) in order to check the goodness of the model outside the mask. Note that the size and shape of the starburst and possible extra features overlapping the galaxy are generally not axisymmetric, so the size and shape of the mask for each galaxy image can be refined after inspecting the residuals, as explained below. Any signs of non-axisymmetric features, such as spiral arms, distortions or possible dust lanes, can be detected in the residual images. The model should be fainter than the galaxy in the starburst region and therefore, the residuals within the masked inner region should be positive.

From the image of residuals, we use *imreplace* to create a new mask by setting to 1 all those pixels whose residual is larger than three times the local rms. In this way, the new mask will generally be smaller and will follow more precisely the shape of the starburst region. We call these new masks *irregular masks*. Then, we fit the image again. This iterative process aims at optimizing P_{area} by adapting the mask to the actual extension and shape of the starburst region. When no significant changes

of the parameters are obtained by refining the masks (typically <1%), and the residuals do not change appreciably, the iterative procedure stops.

In Fig. 1 we show a comparison between the final mask derived from the iterative fits and the continuum-subtracted $H\alpha$ contours ($> 3\sigma$), overlapping the B band image of Mrk 35. The $H\alpha$ emission was useful to give us a first guess mask but it turned out to be somewhat smaller than the whole starburst region in the B band after the complete mask refinement. Thus, relying only on the $H\alpha$ image may lead to an overestimation (albeit small) of the n shape parameter.

6- Definition of Solution

The final solution is obtained by using the irregular masks. Once we determine the stability range as well as refine the mask in shape and size, we choose the best solution as the one with the minimum χ^2_v residuals. This solution is constrained by the dispersion of the stability range and the limits imposed by the possible error sources, as we will discuss later.

4. Simulations

In order to test the reliability of the method and to determine its robustness and flexibility, we carried out a set of fits with synthetic galaxies. Our interest in this exercise is to determine the typical errors induced by the limited number of pixels used in the fit and to study the stability of the fitted parameters as a function of P_{area} . This way, we are able to define a data range within which the procedure provides reliable solutions. We have built a set of model galaxies following the criteria:

- The surface brightness profile was assumed to be a Sérsic law, with two possible values for n : 1 (disk-like objects), and 4 (spheroidal objects). In both cases the ellipticity was set to 0, assuming in all cases a face-on configuration ($q = 1$).
- We simulated the starburst emission as one single burst having a Gaussian profile, concentric with the Sérsic distribution.
- The difference in magnitude between the whole galaxy (host + starburst) and the LSB component was assumed to vary between 0.5 and 1.
- The simulated burst contaminates (by 0.01 mag or more) the radial Sérsic profile between $\sim 0.5 - 2.5$ times R_e .
- We introduce a Poissonian noise and a background sky, generated by the *mknoise* task in IRAF. We used the same read-noise and gain parameters of the real galaxy images in our sample. The synthetic galaxies have then surface brightness limits and signal-to-noise ratios similar to those of the real images.

As an example, two synthetic galaxies, a Sérsic profile with $n = 4$ on the right, and with $n = 1$ on the left, are presented in Fig. 3. Both include a synthetic Gaussian burst overlapping their light distribution up to $P_{\text{area}} = 9$. The circular contours (in black) show the size of some of the applied masks. The outermost isophote (in white) correspond to $1\sigma_{\text{sky}}$, where σ_{sky} is the *rms* background of the image.

We applied the method described in §3 to fit and recover the Sérsic parameters. We ran GALFIT with a first-guess estimate as an initial input. In Figures 4, 5 and 6 we present examples of the results.

We show in Fig. 4 the relative deviation (i.e., the difference between output and input values divided by the input value) in R_e and n , as well as the deviation (i.e., the difference between output and input values) in m_{tot} as a function of R_{mask} (upper scale) and R_{mask}/R_e (bottom scale) for two galaxies described by $n = 1$ (left) and $n = 4$ (right) Sérsic profiles. In this synthetic galaxy, the starburst component contaminates $\sim 35\%$. The last plotted model ($R_{\text{mask}} \sim 23''$) corresponds to $P_{\text{area}} \sim 75$. Red solid lines are models with the sky left as a free parameter. Black solid lines are models with a fixed sky value. The error bars correspond to the statistical uncertainties estimated by the GALFIT χ^2_v minimization. The grey bands indicate deviations of 10% and 20% in the output R_e and n parameters for $n = 1$ and $n = 4$ respectively, and 0.1 mag deviations for m_{tot} in both cases. Lower and upper dashed-lines are models for which the sky was fixed to $\langle \text{sky} \rangle \pm \sigma$, where σ is the sky uncertainty. We obtain reasonable estimations of the sky level ($\sigma \sim 0.2-0.5\%$ sky) when the portion of sky in the frame is large enough, typically ≥ 3 times the diameter of the $1\sigma_{\text{sky}}$ isophote. Two independent methods were applied in order to estimate a value of the sky. In the first, we use the *ellipse* task in IRAF to calculate an extended profile of the galaxy to the edge of the frame. By plotting the flux as a function of radius we can estimate a region where the contribution of the galaxy is negligible and the background can be considered flat. Thus, the median and the standard deviation of the outer points are used (e.g. see Pohlen & Trujillo 2006). The second method is easier and faster; in addition to stars and other background and/or foreground objects, the entire galaxy is masked out to an ellipse with a flux smaller than the *rms* of the background. Thus, we fit with GALFIT only the sky function to the image obtaining $\langle \text{sky} \rangle \pm \sigma$. Both estimations agree for our simulations within ± 0.05 counts ($\sim 0.2\%$ sky).

Fig. 5 shows the comparison between the deviations of the output m_{tot} , R_e and n parameters as a function of R_{mask} (upper scale) and R_{mask}/R_e (bottom scale), for three galaxies with different starburst size. Galaxy with $n = 1$ is to the left while the $n = 4$ galaxy is to the right. Different line colours were used to indicate galaxies with different synthetic starburst size, varying between $\sim 1R_e$ and $2R_e$ ($P_{\text{area}} \sim 17\%$ in black, $\sim 35\%$ in red, and $\sim 50\%$ in green). The error bars and the grey bands have the same meaning as in Fig. 4.

Finally, in Fig. 6 we show the main output parameters (m_{tot} , R_e , and n) versus R_{mask} and R_{mask}/R_e for a compact synthetic disc-like object with a starburst occupying $\sim 50\%$ ($\sim 1.9R_e$) of the pixels until the $1\sigma_{\text{sky}}$ level. The last model ($R_{\text{mask}} = 20$) has $P_{\text{area}} \sim 95$. The horizontal dotted line in the m_{tot} plot corresponds to the total luminosity of the galaxy (host+starburst). Lines as well as deviations and uncertainties have the same meaning as in Fig. 4.

The examples shown in Figs. 4 - 6 illustrate the existence of two features: a sudden change of the parameters, i.e. a significant change of the slope (an elbow), which indicates the region where the starburst becomes practically absent (R_{tran} , in-

indicated by asterisks in the figures), and a range of models (with $R_{\text{mask}} \geq R_{\text{tran}}$) for which the Sérsic parameters are stable within the uncertainties showed by the grey bands.

We resume and discuss our results as follows:

- Our simulations show that the starburst contamination has been clearly discriminated by plotting the successive models with different masks, i.e. *parameters vs. R_{mask}* . The sudden change in the main parameters (m_{tot} , R_e and n) followed by a more or less extended stability region give an estimation of the R_{tran} value. That change is well determined by the elbow in the plot, as shown in the Figures 4 - 6. The Sérsic parameters are recovered within the formal errors from $R_{\text{mask}} = R_{\text{tran}}$. The parameter uncertainties grow up when $R_{\text{mask}} > R_{\text{tran}}$, showing no systematic effects. Models with $R_{\text{mask}} < R_{\text{tran}}$ (i.e, with too small a mask) produce large systematic overestimations in n and luminosity, which also depends on the starburst luminosity. The condition $m_{\text{galaxy}} < m_{\text{host}}$ is a logical (physical) constraint to the solution, as shown in the Fig. 6 (dotted line); in a narrow range of fits, where $R_{\text{mask}} < R_{\text{tran}}$, the luminosity of the host can be brighter than the whole galaxy.

- When we mask the entire starburst, the amount of galaxy pixels with $S/N > 1$ used for the fit is critical in order to recover the Sérsic parameters with small uncertainties (see Figs. 4-6). The errors induced by sky subtraction as well as the random uncertainties estimated from χ^2_{ν} minimization in the model parameters increase with P_{area} , those for $n = 1$ models being smaller than those of $n = 4$ models.

- Besides the starburst contamination, the other possible and critical systematic error source in fitting Sérsic profiles at very faint levels is the measurement of the correct sky value. Relative deviations caused by an erroneous sky subtraction in low n objects are smaller than in higher n objects. The most affected Sérsic parameter is n . For low n objects, we estimate uncertainties within 10% in a significant range of P_{area} for a given combination of model parameters. For high n galaxies that range could be narrower, and errors within 20% to 30% are expected. We estimate ranges of, at least, $\sim 25\text{-}30\%$ R_e in which the parameters are stable within these relative deviations.

- In order to weight the pixels in the fit (with their own noise) GALFIT makes a model from the data information, so accurate solutions require accurate noise information, basically: readnoise, gain, the number of images combined, and sky level. In our simulations we have shown that fits with both fixed and free sky value are in good agreement if the portion of sky is large enough, with uncertainties growing up towards low S/N levels. The χ^2_{ν} minimization uncertainties in fits with a free sky value are greater than in those with a fixed one.

- In our simulations all the parameters behave in a similar way for all the starburst sizes and luminosities considered; e.g, a downward slope followed by a flatter curve. As shown in Fig. 5 the R_{tran} value is well determined in all cases. The range where parameters are stable (grey bands in Figs. 4-6) depends on R_{mask} and on the S/N of the fitted portion of the galaxy. An important result is that our solutions show an acceptable stability in their parameters in the range $R_{\text{mask}}/R_e \leq 2$, with relative deviations growing as the mean S/N ratio of the fitted portion of galaxy decreases. Even when the percentage of masked galaxy is large ($\gtrsim 1.5R_e$), we can still find a range of

stability, $\gtrsim 0.4\text{-}0.5R_e$, with uncertainties between 10% and 20%. For low n galaxies the portion of galaxy required for a good fit is smaller than for high n galaxies, which generally show larger random uncertainties (see Figs. 4-6).

5. On Fitting the LSB Host Galaxy in BCDs

In Paper I we analysed the benefits and drawbacks of fitting a Sérsic law to the starburst-free region of BCDs radial profiles. Here we apply our previous research to fit two-dimensional images with Sérsic profiles. Although it was argued that the Sérsic law provides a reliable description of the host galaxy, we must assess how sensitive the derived two-dimensional Sérsic parameters are to the observational uncertainties.

5.1. Sensitivity to the sampled area

Regardless of the specific technique used to fit a Sérsic model to BCD host galaxies, we must be careful about the choice of the fitted data points (in a radial profile) or number of pixels (in an image), since the Sérsic parameters could be very sensitive to that choice. In Paper I we explored the effect of a limited radial interval in a 1D fit and concluded that accuracy in its selection is crucial for small radial ($R_{\text{tran}} \geq 1\text{-}2$ scale lengths) and surface brightness intervals (typically less than 4 mag). A broad overview of this problem in the simulations of ideal galaxies has already been presented in §4. As was already observed by Makino et al. (1990) for 1D fits, we find that in 2D fits the shape parameter n is also the most sensitive and least constrained parameter, especially when the fit is done on a restricted surface brightness range.

The inner limit of the fitted interval is given by the size and shape of the mask, as parameterized by R_{tran} . Since the starburst emission generally has a steeper light distribution, a small underestimation of R_{tran} will provide significantly higher n values.

Uncertainties in this case can be quantified by means of the dispersion of the output parameters of fits with masks of different sizes. We have tested the procedure through our simulations, taking into account different settings of the input models. In particular, the relationship between R_{tran} , R_{mask} and R_e was studied (see §4). In our sample we found that the stability in the parameters is generally reached when $R_{\text{tran}} \gtrsim R_e$ (see Table 2). This indicates that these galaxies have extended starburst emission, and thus we have to take special care with the size and shape of the masks. The accurate isolation of the starburst emission is the most important strength of the technique.

As shown in the simulations (see §4) the more concentrated the starburst is, the easier it is to find reliable and stable solutions (e.g. Mrk 370, Mrk 36, Tol 127 and Mrk 35).

In those galaxies where the star-forming knots are spread out over the whole galaxy, we could recover information from those inter-knot pixels, increasing the number of pixels being fitted. Although this could be useful to check the stability of solutions, those pixels could have a small starburst light contribution. Thus, an accurate and more reliable solution is obtained when the whole starburst contamination is completely

masked out. Fig. 7 displays an example, using the R -band image of Mrk 86. An irregular mask derived by our procedure (shown in white), masks out only the peaks of the main knots. The fitted parameters are $n = 1.07$, $m_{\text{tot}} = 11.60$ and $r_e = 25.86$ arcsec. The contour of an elliptical mask (shown in yellow) including almost the whole starburst emission is also shown. Fitting the host galaxy with that mask, $n = 1.28$, $m_{\text{tot}} = 11.85$ and $r_e = 31.56$ arcsec are obtained. Notice that when fitting a larger fraction of pixels (i.e. when using the irregular mask) the n value is lower than in the opposite case, but the luminosity is 0.25 mag higher. Although there seems to be still a small amount of starburst contamination, it is evident that the host galaxy of Mrk 86 has a disc-like object structure. Our best fit in the R -band was $n = 1.02$, $m_{\text{tot}} = 11.73$ and $r_e = 25.49$ arcsec, by using a bigger irregular mask (derived from the B -band frame) which isolates the whole starburst emission following its shape.

5.2. Sensitivity to sky subtraction errors

As we have already shown in our simulations the uncertainties resulting from noise fluctuation and sky background subtraction are propagated into the structural parameters when we fit a model to the outer, low signal-to-noise regions of a galaxy. In particular, the Sérsic profile has more extended and shallower tails for high values of n . Thus, an over-subtracted sky background will produce an underestimated n value, while an under-subtraction will overestimate n . We expect that the larger the intrinsic n value, the more sensitive it becomes to this error source (see Paper I and §4).

We analysed the case of Mrk 5 in order to illustrate this error source and compare it with our previous simulations and with a similar example given in Paper I. Results are shown in Table 3. Three cases were examined. First we considered the best sky background subtraction. In the second, we over-subtracted the sky background by about 3 times the sky uncertainty, and in the third we under-subtracted it by the same amount. This is equivalent to fitting two profiles that follow the envelopes of the error bars considered in Fig. 5 of Paper I. For each of the three cases we computed the Sérsic parameters for the final irregular mask ($R_{\text{tran}} = 10.97$ arcsec). The B -band image of Mrk 5 has its best-fit $n = 0.99$ for $R_{\text{tran}} = 10.97$ arcsec (bold row in the Table 3). By under-subtracting the sky background n goes up to 1.17, r_e increases by 9%, while the total luminosity does not change by more than 0.05 mag. Over-subtracting the sky background by the same amount, n falls to 0.88, r_e decreases by 4% and the total luminosity decreases 0.06 mag.

5.3. Other error sources

In the fitting procedure, GALFIT estimates the statistical uncertainties by using the covariance matrix of the parameters (see P02 for a detailed description). Those uncertainties are random errors (Poissonian fluctuations) since GALFIT assumes that the fitted profile is correct, so these estimated errors are generally

very small compared to non-random errors from other sources. For our galaxies, these random errors are $<1\%$.

Galaxies are not perfectly axially symmetric objects. Since GALFIT does not allow for radial changes in axis ratio and position angle of a given component, we expect to obtain larger residuals when fitting regions with twisted or irregular isophotes. This is a remarkable weaknesses of the method. Mrk 35 (see Fig. 10) is useful to illustrate this case. This galaxy shows negative and positive residuals in the border of the mask, just in the region where isophotes twist. However, this does not seem to have a great effect on n , r_e , or m_{tot} values. If we observed systematic residuals produced by these effects, we could check whether they are produced by a real feature (e.g. dust, spiral arms, bars, isophote twists, etc...), and quantify the changes in the parameters by playing with the ellipticity and the position angle, i.e., fixing different values as input in the fits, and comparing its residuals.

5.4. Consistency checks

In order to overcome the above problems and to assess the reliability of the fit, we need to carry out some consistency checks.

First, the reliability of the derived Sérsic parameters are assessed by examining the stability plots. Given their sensitivity to the P_{area} range we explore whether there exists a range in the light profile where the fit is stable and does not depend on the exact choice of R_{tran} . The stability criterion is the same as that applied to the simulations in §4. Second, as we expect that the old stellar host galaxy has negligible color gradients (as shown by the observed behaviour in the outer parts, see for example C01b, Gil de Paz & Madore 2005), both n and R_e should be the same in all passbands, while the differences in μ_e and m_{tot} reflect the LSB colors. Finally, the sky background analysis implemented in our simulations (see §4) is systematically applied.

In Fig. 8 we show the three model parameters (m_{tot} , R_e and n) of Mrk 370 for three bands: B (blue line), V (green line) and R (red line), versus R_{mask} . Each point in the lines corresponds to one fit by using an elliptical mask with a given R_{mask} (and thus, P_{area}) value. We notice some features: first, there exists a sudden change in the slope of the curves by increasing the size of the mask. This “elbow”, as shown in the previous simulations, indicates the region where the starburst becomes practically absent. The second, these free parameters are quite stable (grey bands) in the range between $R_{\text{mask}} \sim 17$ and 28 arcsec. The grey bands correspond to dispersions $\sigma_n = 0.20$, $\sigma_{m_{\text{tot}}} = 0.10$, and $\sigma_{R_e} = 2''$. In the case of n and R_e these bands take into account the dispersion between filters, which can be explained by differences in image depth and quality. We refine the mask by using the positive residuals ($> 3\sigma$) in this range of stability thus obtaining the final irregular masks (see §3). With it, we obtain a better fit, i.e. χ_v^2 , constraining the starburst mask in size and shape. We also perform various fits constraining parameters such as c , PA , q , or the centre coordinates, by varying the input values, and playing with small variations of the sky background in order to check the stability and find the best χ_v^2 and residuals. We indicate the final best fits by the color dots. Notice that for the B filter the difference between the ellipti-

cal masks fits (blue line) and the irregular mask fit (blue dot) is quite large. In a filter where the starburst is more luminous, this result remarks the importance of a better constraint of the size and the shape of the mask.

6. Results

The results of the 2D fitting of a Sérsic law to the starburst-free regions of the galaxy images are presented in Table 2. It is worth mentioning that, in all cases after the procedure is completed, stable parameters were obtained. The consistency checks discussed in §5.4 were applied systematically to all of the galaxies. As can be seen in Table 2, the dispersion in n and r_e between different filters is always less than 10% except for I Zw 123 ($\sim 23\%$ in n). These small discrepancies among different filters are within the uncertainties expected from our simulations and can also be explained in terms of the different quality of the data. For each galaxy, we calculated P_{area} .

We calculate a R_{tran} value as the radius of a circular mask with the same number of pixels as that used for the best fit. In all cases we were able to fit more than 74% of the galaxy pixels. The ratio R_{tran}/R_e varies between 0.70 (Mrk 370R) and 1.73 (I Zw 123V). To estimate the uncertainties in n , r_e and m_{tot} (here m_{LSB}) we compute the dispersion between parameters in the stability range defined for each frame, as well as the difference between the values obtained when fitting with a fixed sky-background and those obtained by setting the sky-background level as a free parameter.

We discuss our results in the following subsections, comparing them with those obtained in Paper I. In Fig. 9 and Fig. 10 we show three images for each galaxy: (left) the galaxy, (center) the Sérsic model, and (right) the residual image, all in logarithmic intensity grey scale.

6.1. Comparison with previous 1D fitting

This paper confirms that low n Sérsic models are able to reproduce, within the uncertainties, the surface brightness distribution in these three pass-bands in all galaxies of the sample. This may indicate that, for this sample, the hosts resemble a disc-like — exponential — structure.

We compared our results with those of Paper I. Fig. 11 shows the model parameters, n , r_e , m_{tot} , and μ_e as well as R_{tran} and the surface brightness evaluated in R_{tran} , extracted by the 2D technique for each galaxy in the three bands: B (blue filled dots), V (green squares), and R (red asterisks), versus the 1D values reported in Paper I. The diagonal line in each plot represents a perfect match between the two sets of values. The main issues are:

- The agreement between the Sérsic parameters in both studies is fairly good for five of the eight galaxies of the sample. However, small differences are found for one galaxy (Mrk 86), while for the other two galaxies, Mrk 5 and I Zw 123, the Sérsic parameters between the two fitting techniques are clearly in disagreement, especially for the n shape parameter (see Fig. 11a). In Paper I their host galaxies are presented as possible spheroidal candidates, being fitted by high n values, $\langle n \rangle_{\text{BVR}} = 2.66$ for Mrk 5 and $\langle n \rangle_{\text{BVR}} = 2.81$ for I Zw 123,

while we obtained $\langle n \rangle_{\text{BVR}} = 1.03$ for Mrk 5 and $\langle n \rangle_{\text{BVR}} = 1.89$ for I Zw 123.

- For all the galaxies, we fitted the images successfully with smaller R_{tran} than in Paper I (see Fig. 11f). We can fit the images not only with a higher number of pixels — crucial to minimize the uncertainties — but with a radial range more extended toward the centre, still avoiding starburst contamination. Here, we reproduce an example presented in Paper I (see their Fig. 2): the stability plots in n , R_e and m_{tot} for Mrk 36 (B band) are shown in Fig. 12 (see caption for details). From the comparison between both techniques, we identify some differences. Firstly, the radial range for which the parameters are quite stable is bigger in the 2D case. Secondly, the final fit isolates the starburst emission more accurately, thus including more high S/N pixels. Finally, the uncertainties are quite smaller than the 1D case.

Furthermore, since it was described in §5.1, n could be poorly constrained when the fit is done in a restricted surface brightness range. We can define the surface brightness interval as the difference between the surface brightness evaluated at R_{tran} (μ_{tran}) and the value at $S/N = 1$ ($\mu_{s/n=1}$). The surface brightness interval is most cases > 4 mag, and > 3 mag for the other cases. Notice that these values are lower limits since GALFIT fits those pixels with $S/N < 1$. We list in Table 2 both μ_{tran} and $\mu_{s/n=1}$.

By the 2D fitting technique we can model the starburst-free region more easily and with higher accuracy, and improve on the stability of the Sérsic parameters, especially n , by reducing the size of the mask and thus providing a larger range of surface brightness available for fitting (see Fig 11d).

6.1.1. Special cases

A special analysis was devoted to Mrk 5 and I Zw 123 (see Fig. 10), whose 1D and 2D parameters show the largest difference (see Fig. 11).

1) Mrk 5. —

By using the *bmodel* task in IRAF we performed 2D modelling of the radial Sérsic profiles obtained in Paper I, taking into account only those isophotes used in the fit. We have subtracted the resulting models from the galaxy image in order to obtain the residuals and compare them with those given by GALFIT. Fig. 13 gives models and residual images in a surface brightness colour scale. The regions shown in grey are pixels masked out from the fit. Quantitatively, both residuals are quite small along the whole LSB component. Residual histograms for both models are shown in Fig. 14. Fig. 14(left) presents the GALFIT residual distribution while Fig. 14(center) shows the residual distribution from the 1D fitting. We normalize the number of pixels by the total number of pixels above a given S/N threshold. We present three levels ordered by increasing total pixel number: $S/N = 2$ (blue), $S/N = 1$ (black) and R_{max} (with $S/N < 1$, in red), where R_{max} is the outer limit for the 1D fitting (from Paper I). In Fig. 14 (right) we show the comparison between both distributions out to R_{max} .

The residuals show a Gaussian distribution centred on 0. As we can observe, by decreasing the S/N threshold the Gaussian becomes broader as we include more low signal-to-noise pixels. As we can see in Fig. 13c, no clear difference is observed between both techniques for the same isophote level. Also, as we showed in Section 5.2 (see also Table 3), the sky background uncertainties in the fit can be well determined. Stable solutions are found only among low n values. This way, we are unable to explain the differences on the Sérsic parameters from the 1D and the 2D techniques.

On the other hand, the inward extrapolation of the best-fitting 1D Sérsic model results in significantly higher luminosity than that observed for the radial profile in the central ~ 10 arcsec (see Fig. 5 in Paper I). Our best-fitting 2D Sérsic model does not show this characteristic. However, if we fit these images with GALFIT, but using the main parameters derived from the 1D fit, i.e., fixing m_{tot} , R_e , and n , we notice the same behaviour again. This fit shows a large negative residual feature inside the entire masked region, with the LSB component brighter than the actual galaxy light distribution.

2) IZw 123. –

We analysed the possible differences between both results by inspecting the residuals and all possible uncertainties in the fit, and we found possible explanations in terms of both the seeing effects and the limited radial interval for fitting.

The images of IZw 123 have a FWHM of about 2 arcsec. In Paper I we fit the radial profile with $r_e = 2.07$, $n = 2.61$, $m_{\text{tot}} = 15.19$ and $r_e = 2.74$, $n = 3.01$, and $m_{\text{tot}} = 14.84$ in B and V bands respectively. In this work r_e is 4.59 and 4.11, n 1.58 and 2.20, and m_{tot} 16.08 and 15.46, in B and V respectively. If we fit the same images in the same conditions but do not use the convolution in the models, r_e goes down to 2.89 and 2.51, n increases to 2.40 and 3.15, while m_{tot} decreases to 15.60 and 14.86, in B and V respectively. These differences show that seeing convolution of the model is important when fitting small galaxies observed in poor seeing conditions.

On the other hand, I Zw 123 has the largest R_{tran}/R_e ratio, i.e., it has the starburst emission with the largest spatial extent, measured in terms of the host galaxy's structural parameters. If it also has a steep Sérsic profile and taking into account the results shown in the simulations (see §4), the resulting parameters could be very sensitive to exactly excluding the starburst emission and to the limited sampled area (see also §5.1). Figure 15 presents the three model parameters, n , r_e and m_{tot} , as a function of R_{mask} in the B band. There is only a narrow radial interval, $7 \lesssim R_{\text{mask}} \lesssim 11$, for which the parameters became reasonably stable, especially for n . Dots with error bars indicates the final best fits, where $R_{\text{mask}} = R_{\text{tran}}$, while asterisks indicates the results from Paper I. The horizontal dashed-dotted line in the m_{tot} plot indicates the magnitude of the whole galaxy (host + starburst); host luminosities brighter than that are physically meaningless.

Comparing the results from both techniques, we propose our best-fitting 2D Sérsic model as the more physically reliable solution, for the outer regions of the LSB host.

7. Summary and final conclusions

We have presented a new two-dimensional fitting methodology devoted to the characterization of the LSB component in BCD galaxies. The technique is based on the GALFIT algorithm developed by Peng et al. 2002, which permits to fit the whole galaxy image after suitably masking out the pixels contaminated by the starburst.

We described the different steps in our methodology. We carried out a set of fits using synthetic galaxies in order to validate the method and to determine its robustness and estimate the associated uncertainties. The method was applied to the eight BCD galaxies already analysed in Paper I. We fit the same dataset, consisting of deep BVR images, using a Sérsic law. Finally, we analysed our results in terms of the possible error sources and we performed a set of consistency checks comparing the results with those of Paper I. We paid special attention to Mrk 5 and I Zw 123.

The main results of this work can be summarized as follows:

1. Our simulations test the robustness of the methodology, and show that the uncertainties in recovering stable Sérsic parameters can be measured in terms of the percentage of how many pixels are fitted relative to the total number of pixels above a given signal-to-noise ratio. Low n synthetic galaxies are characterized by more stable Sérsic parameters and smaller uncertainties compared to high n synthetic galaxies. The shape parameter, n , is the most affected by the uncertainties. The 2D Sérsic parameters of galaxies with R_{tran}/R_e ratios between 0.5 and 2.5 are recovered within typical deviations of about 10% and 20% for low and high n galaxies respectively, if we use — at least — the 50% of the galaxy pixels with $S/N > 1$.
2. All the sampled galaxies show generally stable fits when using more than 74% of the pixels with $S/N > 1$. Sérsic indexes n and effective radii for all the objects show good agreement (within the uncertainties) in the three bands. The eight galaxies present a red LSB component and low n values, suggesting that the LSB hosts of this sample of BCDs share similar structural properties. Seven of them have near exponential light distributions (very close to 1), while the other one has n values close to 2. The uncertainties, estimated from the dispersion in the stability range and those from sky subtraction, are in all cases but one lower than 30%.
3. The mean advantage of the 2D technique over the 1D technique is that we can maximize the fitted portion of the galaxy. Especially in those galaxies with irregular starburst we can accomplish this by using masks that follow the actual shape of the starburst emission. Furthermore, we have been able to put constraints to the sky background uncertainties, which play an important role in the Sérsic parameter errors. Also, we have paid attention to the seeing effects when fitting a small galaxy.

Because of the difficulties of the problem, it is indispensable to work with a homogeneous data set, using the same reduction process and deriving the structural parameters with a

well defined methodology, taking into account all the possible error sources. This two-dimensional technique can provide an important improvement in this kind of analysis.

Acknowledgements. Based on observations made at the Nordic Optical Telescope (NOT), in the Spanish Observatory del Roque de los Muchachos of the Instituto de Astrofísica de Canarias and on observations taken at the German/Spanish Calar Alto Observatory. This work has been partially funded by the Spanish DGCyT, grant AYA2004-08260-C03-01. Thanks are given by R.O.A. to Adriana Caldez and M. Dobrinčić for revising the English. R.O.A. thanks R. Sánchez-Janssen for very stimulating discussions and helpful comments. We are sincerely grateful to Dr. Richer for his very detailed comments, suggestions and time which helped us to improve the quality of the manuscript.

References

- Aguerri, J. A. L., Iglesias-Páramo, J., Vílchez, J. M., Muñoz-Tuñón, C., & Sánchez-Janssen, R. 2005, *AJ*, 130, 475
- Athanassoula, E., Morin, S., Wozniak, H., Puy, D., Pierce, M. J., Lombard, J., & Bosma, A. 1990, *MNRAS*, 245, 130
- Baggett, W. E., Baggett, S. M., & Anderson, K. S. J. 1998, *AJ*, 116, 1626
- Barden, M., et al. 2005, *ApJ*, 635, 959
- Bergvall, N. & Östlin, G. 2002, *A&A*, 390, 891
- Burstein, D. & Heiles, C. 1984, *ApJS*, 54, 33
- Cairós, L. M., Vílchez, J. M., González-Pérez, J. N., Iglesias-Páramo, J., & Caon, N. 2001a, *ApJS*, 133, 321 (C01a)
- Cairós, L. M., Caon, N., Vílchez, J. M., González-Pérez, J. N., & Muñoz-Tuñón, C. 2001b, *ApJS*, 136, 2 (C01b)
- Cairós, L. M., Caon, N., García-Lorenzo, B., Vílchez, J. M., & Muñoz-Tuñón, C. 2002, *ApJ*, 577, 164
- Cairós, L. M., Caon, N., Papaderos, P., Noeske, K., Vílchez, J. M., García-Lorenzo, B., & Muñoz-Tuñón, C. 2003, *ApJ*, 593, 312
- Cairós, L. M. 2000, PhD Thesis, University of La Laguna: "Formation and Evolution of Blue Compact Dwarf Galaxies"
- Caon, N., Cairós, L. M., Aguerri, J. A. L., & Muñoz-Tuñón, C. 2005, *ApJS*, 157, 218 (Paper I)
- Caon, N., Capaccioli, M., & D'Onofrio, M. 1993, *MNRAS*, 265, 1013
- Davies, J. I. & Phillipps, S. 1988, *MNRAS*, 233, 553
- de Jong, R. S. 1996, *A&AS*, 118, 557
- Dong, X. Y., & De Robertis, M. M. 2006, *AJ*, 131, 1236
- Doublier, V., Caulet, A., & Comte, G. 1999, *A&AS*, 138, 213
- Doublier, V., Comte, G., Petrosian, A., Surace, C., & Turatto, M. 1997, *A&AS*, 124, 405
- Fanelli, M. N., O'Connell, R. W., & Thuan, T. X. 1988, *ApJ*, 334, 665
- Gil de Paz, A., & Madore, B. F. 2005, *ApJS*, 156, 345
- Graham, A., Lauer, T. R., Colless, M., & Postman, M. 1996, *ApJ*, 465, 534
- Graham, A. W., & Guzmán, R. 2003, *AJ*, 125, 2936
- Kunth, D., Maurogordato, S., & Vigroux, L. 1988, *A&A*, 204, 10
- Loose, H.-H., & Thuan, T. X. 1986, *ApJ*, 309, 59
- Makino, J., Akiyama, K., & Sugimoto, D. 1990, *PASJ*, 42, 205
- Marlowe, A. T., Meurer, G. R., Heckman, T. M., & Schommer, R. 1997, *ApJS*, 112, 285
- Marlowe, A. T., Meurer, G. R., & Heckman, T. M. 1999, *ApJ*, 522, 183
- Noeske, K. G., Papaderos, P., Cairós, L. M., & Fricke, K. J. 2003, *A&A*, 410, 481
- Noeske, K. G., Papaderos, P., Cairós, L. M., & Fricke, K. J. 2005, *A&A*, 429, 115
- Noeske, K. G., Koo, D. C., Phillips, A. C., Willmer, C. N. A., Melbourne, J., Gil de Paz, A., & Papaderos, P. 2006, *ApJ*, 640, L143
- Papaderos, P., Loose, H.-H., Thuan, T. X., & Fricke, K. J. 1996a, *A&AS*, 120, 207
- Papaderos, P., Loose, H.-H., Fricke, K. J., & Thuan, T. X. 1996b, *A&A*, 314, 59
- Peng, C. Y., Ho, L. C., Impey, C. D., & Rix, H.-W. 2002, *AJ*, 124, 266 (P02)
- Press, W. H., Teukolsky, S. A., Vetterling, W. T., & Flannery, B. P. 1997, *Numerical Recipes in C* (Cambridge Univ. Press)
- Prieto, M., Aguerri, J. A. L., Varela, A. M., & Muñoz-Tuñón, C. 2001, *A&A*, 367, 405
- Pohlen, M., & Trujillo, I. 2006, *A&A*, 454, 759
- Sánchez, S. F., et al. 2004, *ApJ*, 614, 586
- Sargent, W. L. W. & Searle, L. 1970, *ApJ*, 162, L155
- Schlegel, D. J., Finkbeiner, D. P., & Davis, M. 1998, *ApJ*, 500, 525
- Sersic, J. L. 1968, Cordoba, Argentina: Observatorio Astronomico, Univ. Nac. Cordoba
- Silich, S., & Tenorio-Tagle, G. 2001, *ApJ*, 552, 91
- Telles, J. E. 1995, Ph.D. Thesis, Univ. Cambridge
- Tenorio-Tagle, G., Silich, S., & Muñoz-Tuñón, C. 2003, *ApJ*, 597, 279
- Thuan, T. X. 1985, *ApJ*, 299, 881
- Treu, T., et al. 2005, *ApJ*, 633, 174
- Trujillo, I., Aguerri, J. A. L., Cepa, J., & Gutiérrez, C. M. 2001a, *MNRAS*, 321, 269
- Trujillo, I., Aguerri, J. A. L., Cepa, J., & Gutiérrez, C. M. 2001b, *MNRAS*, 328, 977
- Vaduvescu, O., Richer, M. G., & McCall, M. L. 2006, *AJ*, 131, 1318
- Young, C. K., & Currie, M. J. 1994, *MNRAS*, 268, L11

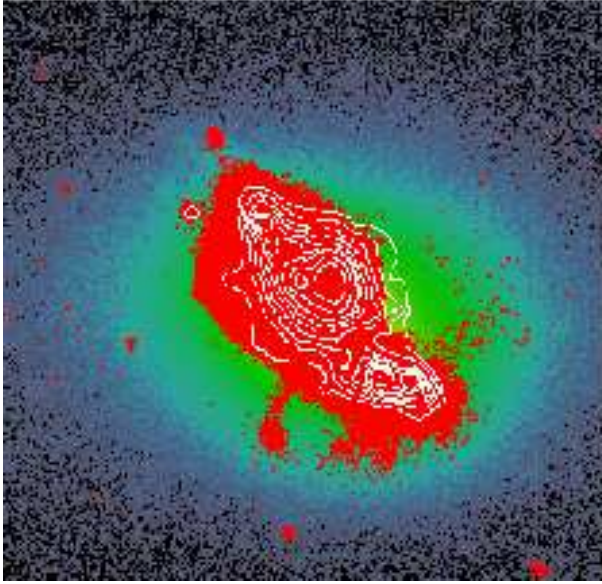


Fig. 1. Mrk 35, *B* band. Overlapped in red, the final mask. In white, the $H\alpha$ contours.

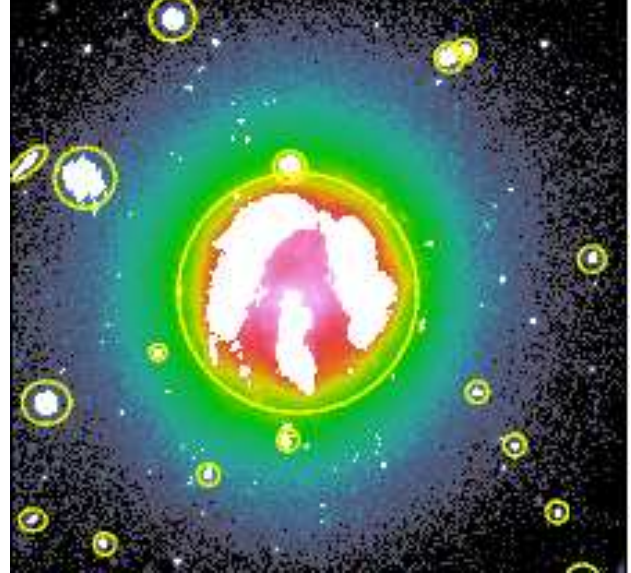


Fig. 7. Mrk 86, *R* band. In white, the mask covering the starburst peaks. In yellow, the contours of the elliptical mask containing most of the starburst emission.

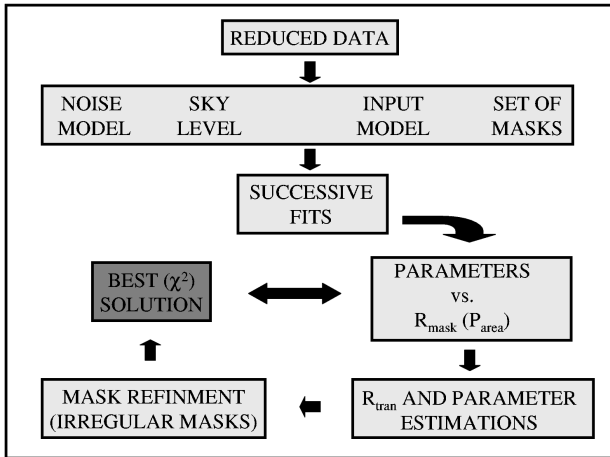


Fig. 2. Scheme showing the main steps of the method.

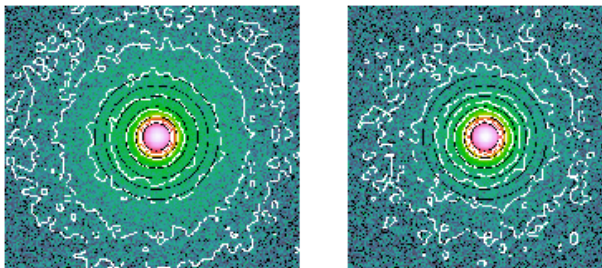


Fig. 3. Two synthetic galaxies with Sérsic index $n = 1$ (left) and $n = 4$ (right). The outermost isophote corresponds to $1\sigma_{\text{sky}}$ (in white), $1\sigma_{\text{sky}}$ being the *rms* of the sky-background. Circular isocontours, overlapped in black, represent the set of masks used in successive fits.

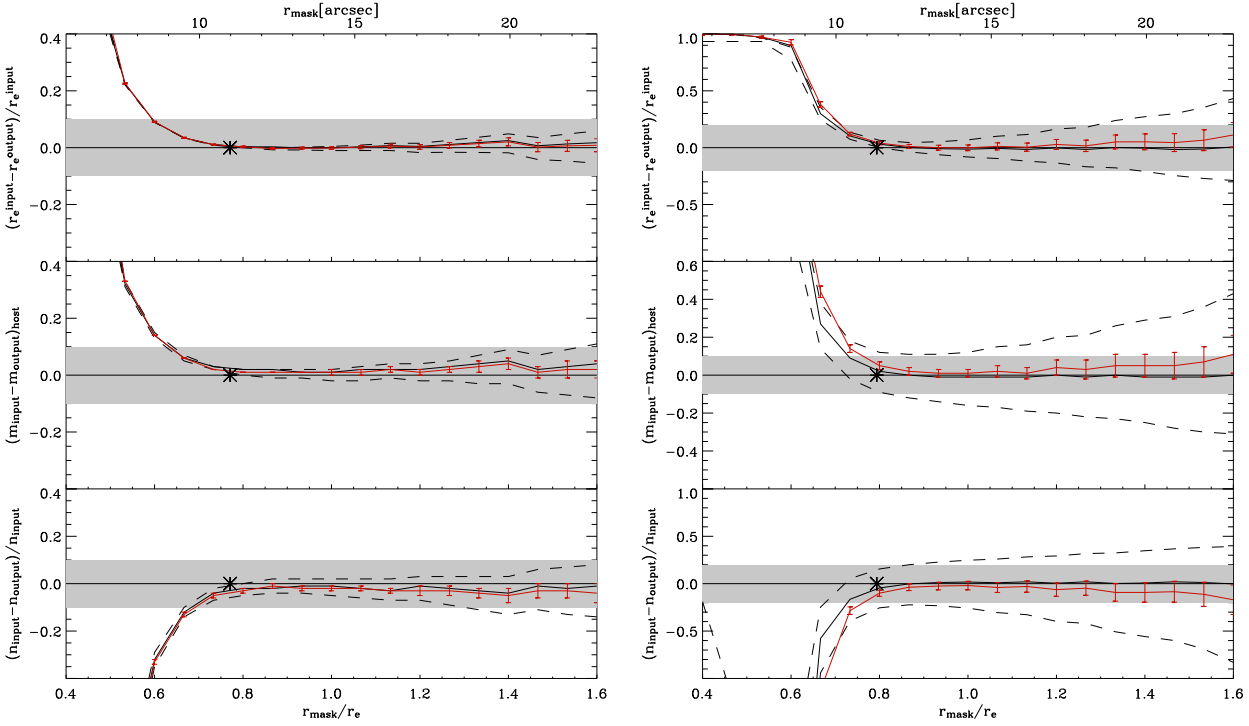


Fig. 4. Relative deviations in the three model parameters (R_e , n and m_{tot}) as a function of R_{mask} (upper scale) and R_{mask}/R_e (bottom scale). To the left we show results for $n=1$ models, while $n=4$ models are presented to the right. Models fitted with a sky value free to vary are represented by solid red lines, while models fitted with a fixed sky value are shown by black solid lines. Lower and higher dashed lines show those models for which the sky was fixed to $\langle \text{sky} \rangle \pm \sigma$, where $\langle \text{sky} \rangle$ is the best sky estimation and σ the sky uncertainty. The grey band indicates deviations of the 10% and 20% for recovered R_e and n parameters in the $n = 1$ and $n = 4$ cases respectively, while 0.1 mag deviations for m_{tot} in both cases. Asterisks in all cases show an estimation of the transition radius (R_{tran}).

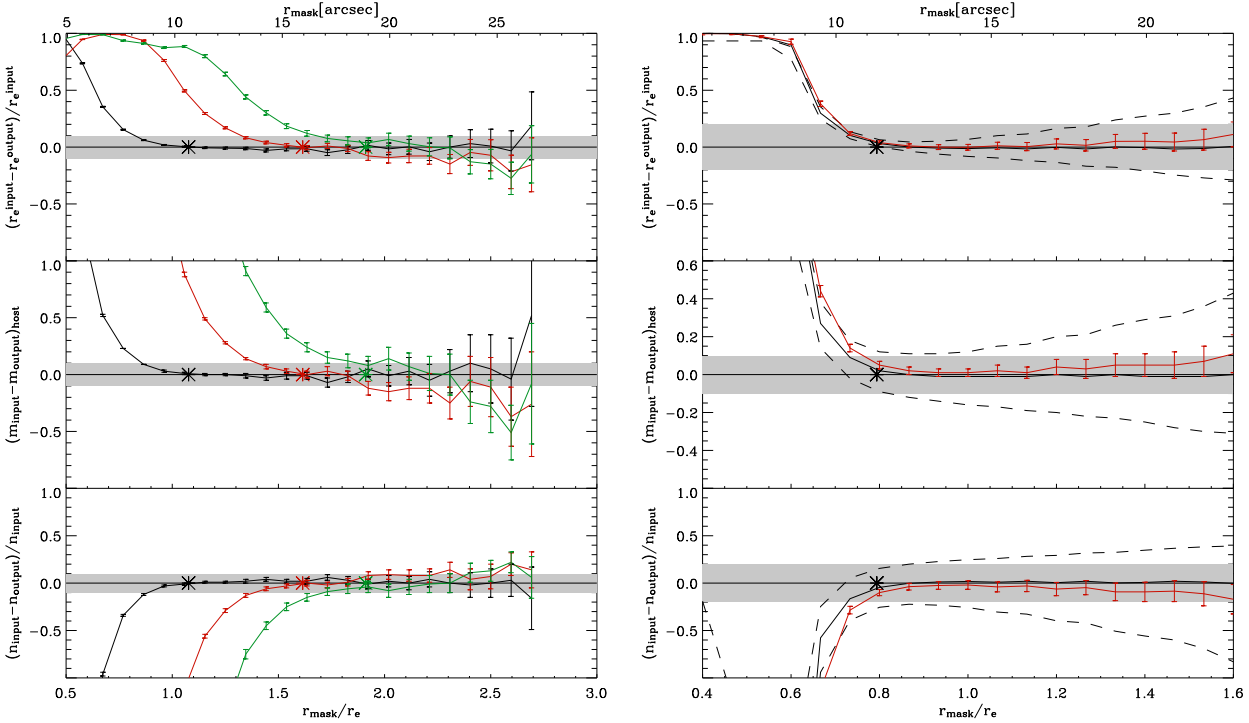


Fig. 5. Relative deviations in R_e , n and m_{tot} as a function of R_{mask} (top) and R_{mask}/R_e (bottom), and the simulated starburst size. Lines show Sérsic recovered models in $n = 1$ (left panel) and $n = 4$ (right panel) in synthetic galaxies for which the starburst size is $\sim R_e$ (black), $\sim 1.5R_e$ (red), and $\sim 2R_e$ (green). Asterisks in all cases show an estimation of the transition radius (R_{tran}).

Table 1. The galaxy sample

Galaxy (1)	Other names (2)	RA(J2000) (3)	Dec.(J2000) (4)	D (Mpc) (5)	A_B (mag) (6)	m_B (mag) (7)	M_B (mag) (8)
Tololo 0127-397		01 29 15.8	-39 30 37	61.0	0.067	16.18	-17.75
Mrk 370	NGC 1036, UGC 02160	02 40 29.0	19 17 50	10.9	0.399	13.19	-16.99
Mrk 5	UGCA 130	06 42 15.5	75 37 33	14.0	0.364	15.22	-15.51
Mrk 86	NGC 2537, UGC 04274	08 13 14.7	45 59 26	8.1	0.232	12.18	-17.37
Mrk 35	Haro 3, NGC 3353	10 45 22.4	55 57 37	15.6	0.031	13.18	-17.79
Mrk 36	Haro 4, UGCA 225	11 04 58.5	29 08 22	10.4	0.131	15.25	-14.84
I Zw 123	UGCA 410, Mrk 487	15 37 04.2	55 15 48	12.5	0.062	15.40	-15.09
Mrk 314	NGC 7468, UGC 12329	23 02 59.2	16 36 19	28.9	0.383	13.78	-18.53

Notes.— Columns: (1) name of the galaxy; (2) other designations of the galaxies; (3) right ascension in hours, minutes and seconds; (4) declination in degrees, arcminutes and arcseconds; (5) distance, computed assuming a Hubble flow with a Hubble constant $H_0 = 75 \text{ km s}^{-1} \text{ Mpc}^{-1}$, after correcting recession velocities relative to the centroid of the local group for Virgocentric infall; (6) extinction coefficient in the B band, from Schlegel, Finkbeiner, & Davis (1998); (7) asymptotic magnitude in the B band, from C01b. Notice that the asymptotic magnitudes listed in C01b were corrected for Galactic extinction following Burstein & Heiles (1984); here they have been recomputed using the Schlegel, Finkbeiner, & Davis (1998) extinction values; (8) absolute magnitude, obtained from the B asymptotic magnitudes using the distances tabulated in (5).

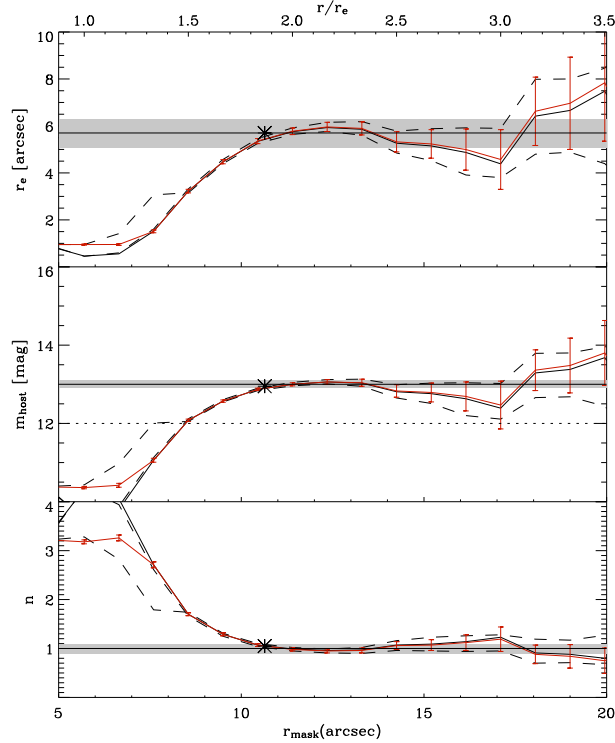


Fig. 6. Example of stability plots: R_e , n and m_{tot} , as a function of R_{mask} and R_{mask}/R_e , for a $n=1$ synthetic galaxy. Models fitted with a sky value free to vary are represented by solid red lines, while models fitted with a fixed sky value are shown by black solid lines. Lower and higher dashed lines show those models for which the sky was fixed to $\langle \text{sky} \rangle \pm \sigma$, where $\langle \text{sky} \rangle$ is the best sky estimation and σ the sky uncertainty. The grey band indicates deviations of the 10% on R_e and n , while 0.1 mag deviations for m_{tot} . Asterisks show an estimation of the transition radius (R_{tran}).

Table 2. Parameters for the LSB host galaxy derived from the Sérsic fit

Galaxy	Filter	$P_{\text{area}}(\%)$	PA	$q(=b/a)$	c	R_{tran}	$R_{\text{tran}}^{\text{1D}}$	n	σ_n	r_e	σ_{r_e}	m_{LSB}	$\sigma_{m_{\text{LSB}}}$	M_{LSB}	μ_e	μ_{tran}	$\mu_{S/N=1}$
(1)	(2)	(3)	(4)	(5)	(6)	(7)	(8)	(9)	(10)	(11)	(12)	(13)	(14)	(15)	(16)	(17)	(18)
Tol 0127-397	<i>B</i>	13.2	-53.8	0.69	0.23	4.58	7.22	1.11±0.19	0.21	4.02±0.80	0.15	17.42±0.19	0.13	-16.51	22.78	23.04	27.06
	<i>V</i>	14.2	-50.5	0.67	0.08	4.75	7.16	0.94±0.15	0.20	4.62±0.72	0.75	16.08±0.20	0.20	-17.85	21.64	21.69	25.95
	<i>R</i>	14.7	-50.8	0.66	0.08	5.27	7.20	1.02±0.24	0.20	4.75±0.24	0.20	15.96±0.21	0.19	-17.97	21.60	21.80	25.98
Mrk 370	<i>B</i>	15.0	-14.8	0.79	0.09	19.20	35.65	1.04±0.08	0.20	23.36±1.00	1.41	13.88±0.13	0.12	-16.31	23.18	22.85	26.42
	<i>V</i>	15.4	-18.4	0.81	0.09	17.65	35.62	1.00±0.10	0.22	23.21±1.54	0.70	13.24±0.10	0.11	-16.95	22.53	22.10	25.63
	<i>R</i>	10.4	-14.0	0.80	0.08	16.80	35.50	1.03±0.14	0.14	23.89±1.33	1.18	12.71±0.10	0.10	-17.48	22.07	21.52	25.49
Mrk 5	<i>B</i>	10.9	13.1	0.76	0.10	10.97	13.78	0.99±0.15	0.38	9.62±1.25	0.61	16.02±0.20	0.14	-14.71	23.33	23.58	28.20
	<i>V</i>	9.6	13.2	0.75	0.07	10.97	13.67	1.05±0.14	0.30	9.53±0.43	1.63	15.54±0.08	0.27	-15.19	22.84	23.12	27.56
	<i>R</i>	9.0	12.5	0.78	-0.01	10.61	13.64	1.05±0.25	0.32	9.53±0.28	0.16	15.21±0.08	0.06	-15.52	22.55	22.76	27.39
Mrk 86	<i>B</i>	18.9	-21.2	0.91	0.00	34.80	45.97	0.94±0.34	0.03	25.65±5.00	0.21	13.10±0.27	0.02	-16.44	22.71	23.35	27.30
	<i>V</i>	16.0	-23.7	0.92	0.01	34.80	45.52	1.00±0.32	0.05	26.24±3.94	0.95	12.31±0.20	0.05	-17.23	22.01	22.60	26.44
	<i>R</i>	14.6	-21.3	0.90	0.00	34.80	46.33	1.02±0.26	0.25	25.49±6.92	5.36	11.73±0.30	0.21	-17.81	21.35	22.01	26.15
Mrk 35	<i>B</i>	20.2	74.0	0.72	-0.02	20.80	24.57	0.99±0.18	0.11	15.30±1.58	0.07	14.15±0.18	0.05	-16.82	22.41	23.06	27.50
	<i>V</i>	17.6	77.3	0.71	0.03	19.45	24.37	1.01±0.27	0.23	14.83±1.43	1.12	13.41±0.15	0.23	-17.56	21.59	22.16	27.71
	<i>R</i>	18.5	77.7	0.70	-0.01	19.45	24.08	0.97±0.16	0.08	14.94±1.13	0.28	13.11±0.12	0.08	-17.86	21.28	21.82	27.88
Mrk 36	<i>B</i>	26.5	-25.9	0.47	-0.00	10.15	12.18	1.00±0.04	0.17	8.79±0.80	0.18	16.92±0.15	0.04	-13.17	23.52	23.80	27.76
	<i>V</i>	26.0	-24.4	0.48	-0.12	10.34	12.39	1.07±0.13	0.12	8.64±0.65	0.40	16.34±0.25	0.05	-13.72	22.98	23.34	26.41
	<i>R</i>	26.5	-23.8	0.49	-0.10	10.34	12.07	1.05±0.08	0.06	8.81±0.72	0.03	15.95±0.10	0.04	-14.14	22.62	22.93	26.84
1 Zw 123	<i>B</i>	17.5	-51.1	0.92	-0.26	7.13	9.17	1.58±0.20	0.18	4.59±0.65	0.50	16.08±0.20	0.06	-14.40	22.21	23.20	27.59
	<i>V</i>	20.0	-52.9	0.89	-0.20	7.13	9.07	2.20±0.17	0.22	4.11±0.37	0.15	15.46±0.14	0.04	-15.02	21.48	22.74	26.68
Mrk 314	<i>B</i>	13.5	14.8	0.77	-0.46	10.80	16.85	1.01±0.17	0.30	9.54±0.79	0.70	14.77±0.11	0.15	-17.53	22.08	22.32	25.95

Notes.— Columns (1) name of the galaxy; (2) filter; (3) relative percentage area (see definition in 3.1.4); (4) position angle; (5) ellipticity; (6) boxy/discy shape parameter; (7) 2D transition radius ($''$); (8) 1D transition radius ($''$); (9) 2D fit Sérsic shape parameter; (10) uncertainty in the shape parameter due to sky subtraction errors; (11) effective radius ($''$); (12) uncertainty in effective radius ($''$) due to sky subtraction errors; (13) total magnitude of the LSB host (mag); (14) uncertainty in total magnitude of the LSB host (mag) due to sky-subtraction errors; (15) absolute magnitude of the host derived from the 2D fit; (16) effective surface brightness (mag arcsec $^{-2}$); (17) surface brightness of the 2D model at its transition radius (mag arcsec $^{-2}$); (18) surface brightness of the 2D model at its $S/N = 1$ level (mag arcsec $^{-2}$).

Uncertainties in columns 10, 12 and 14, are estimated as described in Section 4.

Sensitivity of Sérsic parameters of Mrk 5 (*B*) to changes in the sky background

Sky background	R_{tran}	P_{area} (%)	n	r_e	μ_e	m_{tot}	χ^2_{ν}
Correct sky	10.97	10.9	0.99	9.62	23.63	16.02	2.232
Sky over-subtracted	10.97	10.9	0.88	9.23	23.54	16.08	3.093
Sky undersubtracted	10.97	10.9	1.17	10.47	23.83	15.97	3.013

Table 3. Columns: (2) transition radius (arcsec); (3) masked area relative to $1\sigma_{\text{sky}}$ of the galaxy; (4) Sérsic shape parameter; (5) effective radius ("); (6) effective surface brightness (mag arcsec $^{-2}$); (7) total magnitude of the LSB component derived from the fit (mag); (8) χ^2_{ν} . In bold the best fitting parameters.

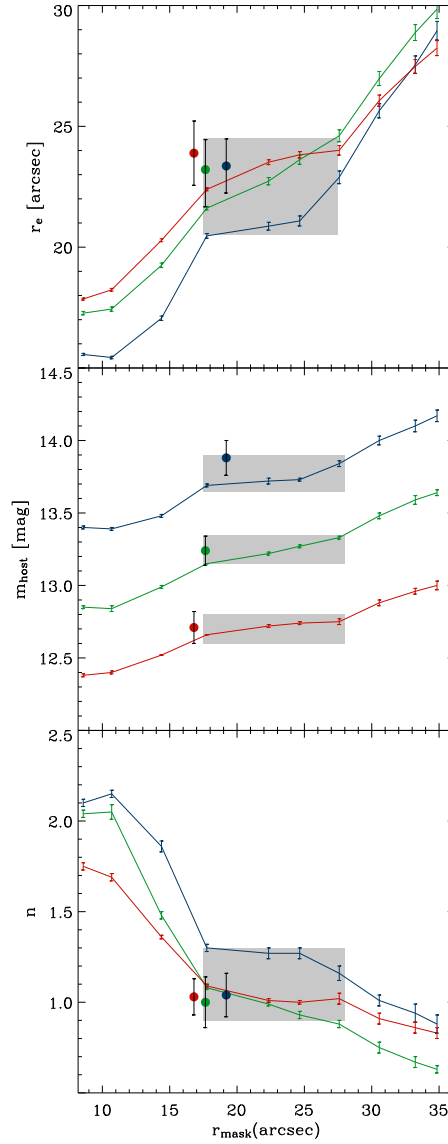


Fig. 8. Stability in the 2D fit of Mrk 370: the free parameters R_e , m_{tot} and n , are plotted as a function of R_{mask} in the three bands (blue=*B*, green=*V*, and red=*R*). Dots in colour are the final best fits. Their error bars take into account uncertainties from the sky subtraction. Grey bands indicates the stability region considered.

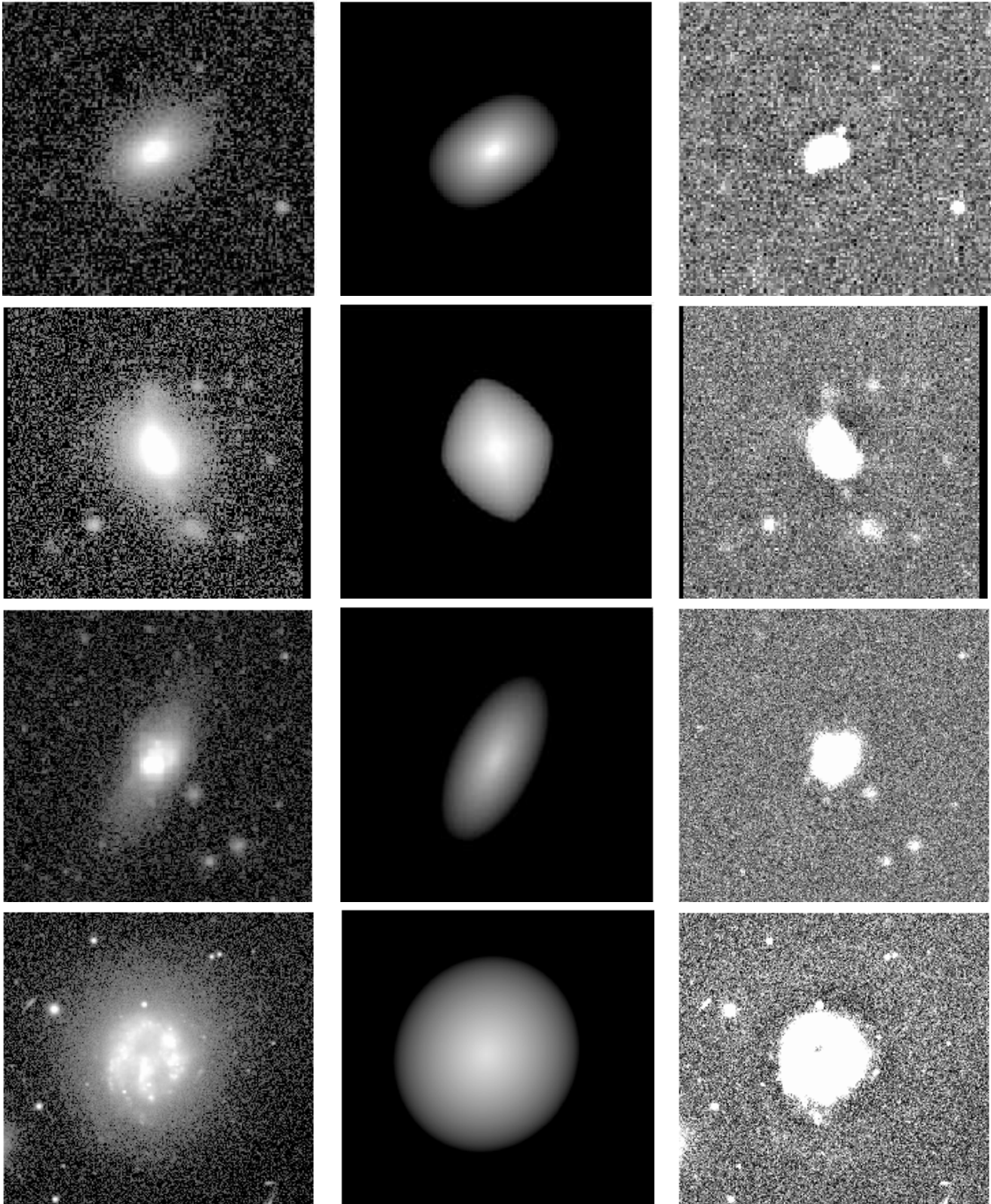


Fig. 9. The galaxy (*Left*) and the Sérsic model (*centre*) in logarithmic intensity grey scale. The residual image (*right*), in linear grey scale for Tol 127 *B*, Mrk 314 *B*, Mrk 36 *B*, and Mrk 86 *B*.

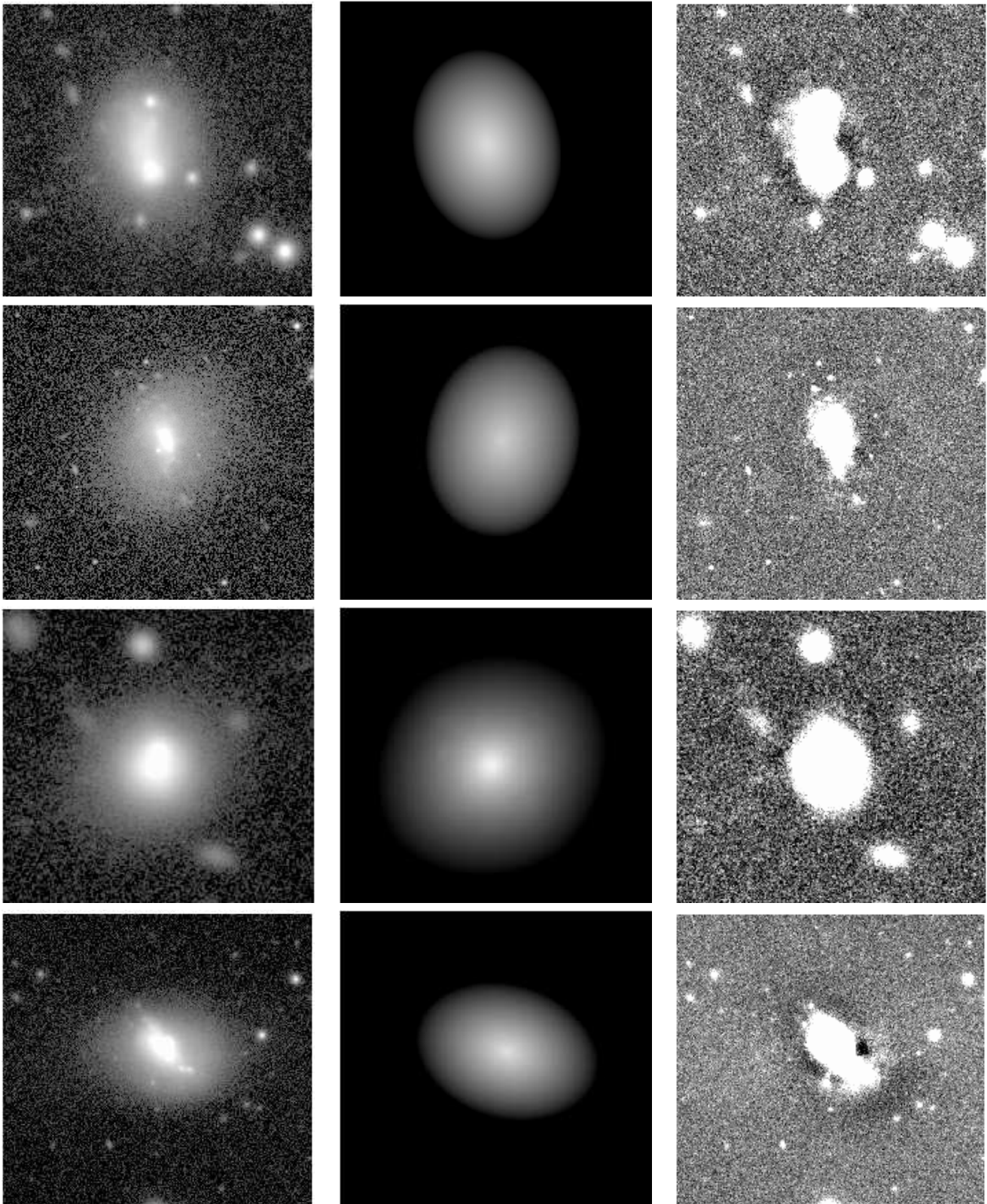


Fig. 10. The galaxy (*Left*) and the Sérsic model (*centre*) in logarithmic intensity grey scale. The residual image (*right*) in linear grey scale for Mrk 5 *B*, Mrk 370 *B*, I Zw 123 *B*, and Mrk 35 *B*.

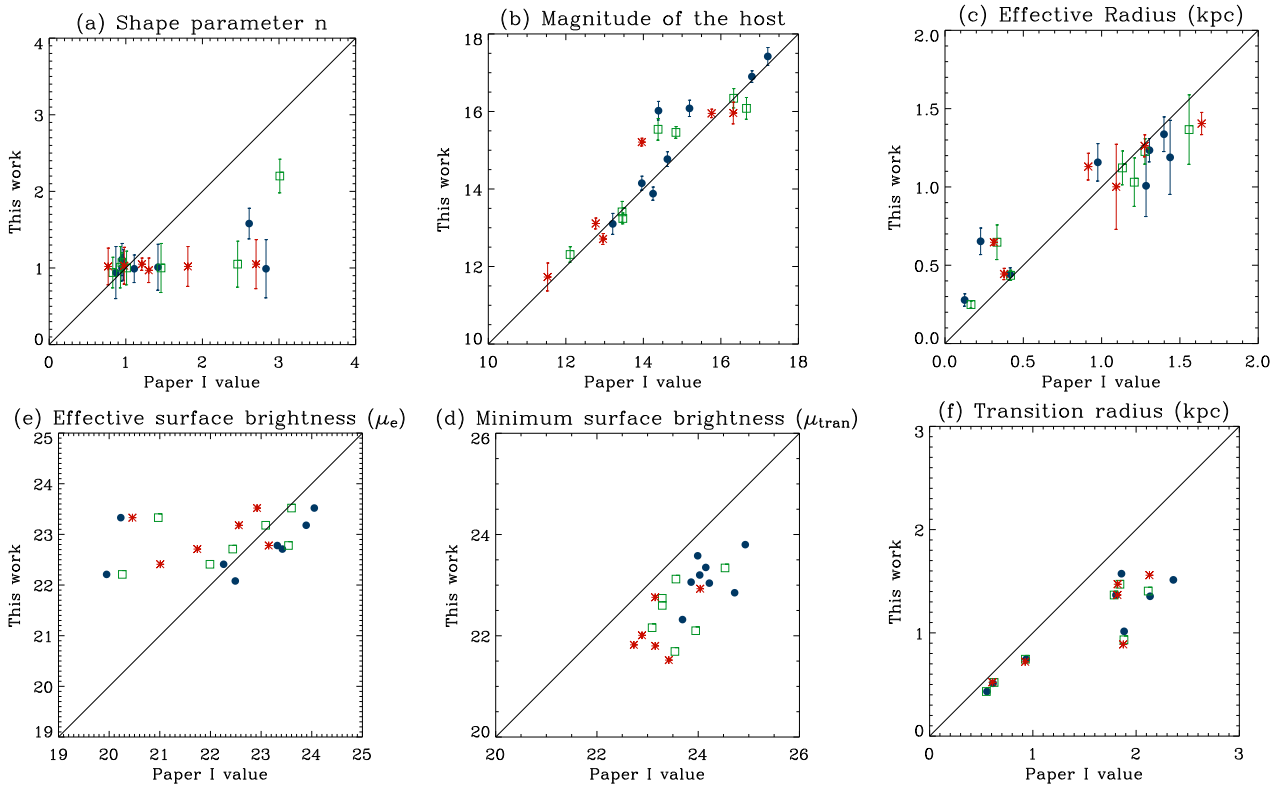


Fig. 11. Comparison between the Sérsic parameters in the three bands (blue dots= B , green squares= V , and red asterisks= R) derived in this work with those reported in Paper I: a) shape parameter n , b) LSB host total magnitude, c) effective radii (kpc), d) effective surface brightness (mag arcsec^{-2}), e) minimum surface brightness (mag arcsec^{-2}), and f) transition radius (kpc).

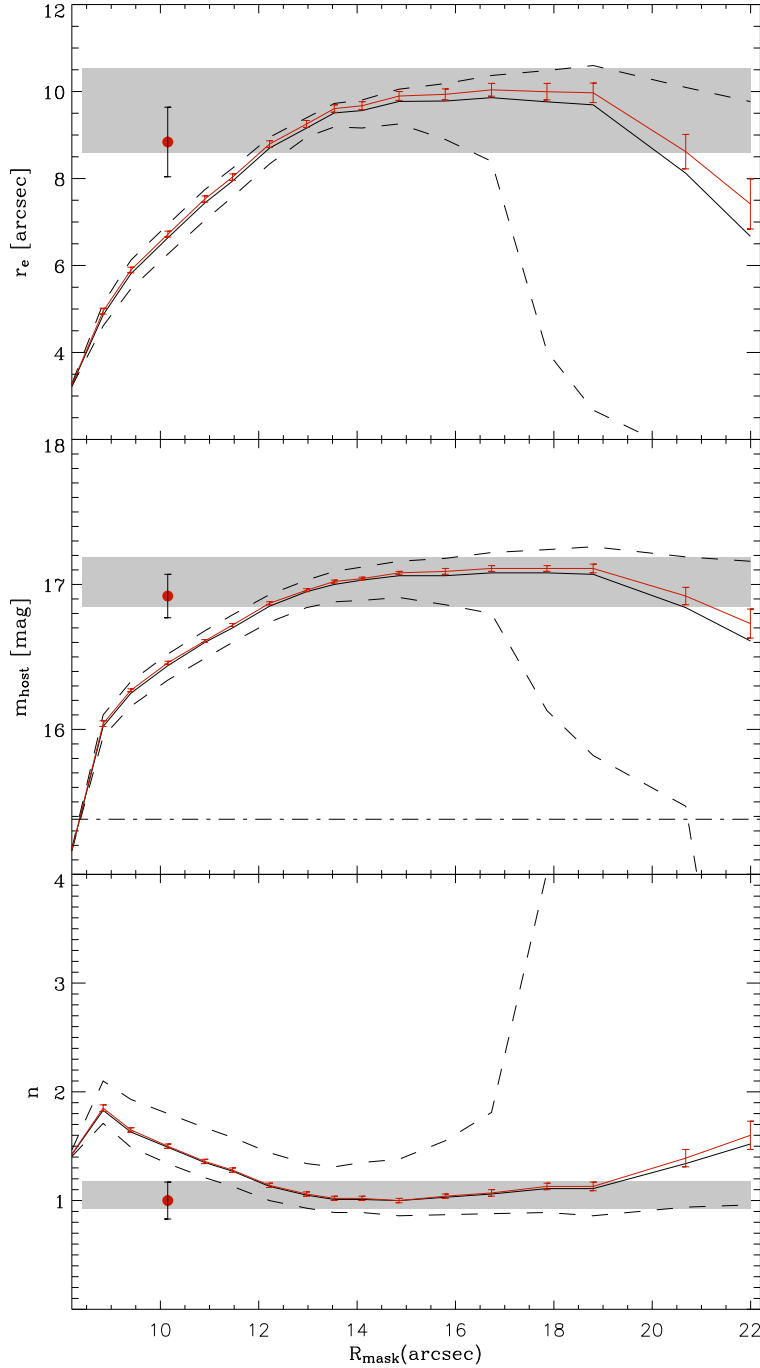


Fig. 12. Stability in the 2D fit of Mrk 36 (B band): the parameters R_e , m_{tot} and n , are plotted as a function of R_{mask} in the B band. Red lines indicates fits for which the sky-background was a free parameter. Black lines indicates fits with a fixed sky-background level in our best estimation. The error bars (only statistical uncertainties) were put only in the red curve since they are the bigger. Dashed lines indicates fits with a fixed sky-background in $\langle \text{sky} \rangle \pm \sigma$, where σ is the uncertainty in the sky estimation. Dots are the final fits. The horizontal dashed-dotted line in the m_{tot} plot indicates the magnitude of the whole galaxy (host + starburst). Their error bars represent the quadratic sum of uncertainties from both dispersion in the stability range and from the sky subtraction (see text for details). We notice that there is a radial interval, $12 \leq R_{\text{mask}} \leq 19$, within which the Sérsic parameters are quite stable in the range indicated by the grey band (with deviations of $\sim 1''$ in R_e , ~ 0.17 in m_{tot} , and ~ 0.14 in n). Our best fits are within the uncertainties and have a transition radius (when $R_{\text{mask}} = R_{\text{tran}}$) significantly smaller than those obtained by using the elliptical masks.

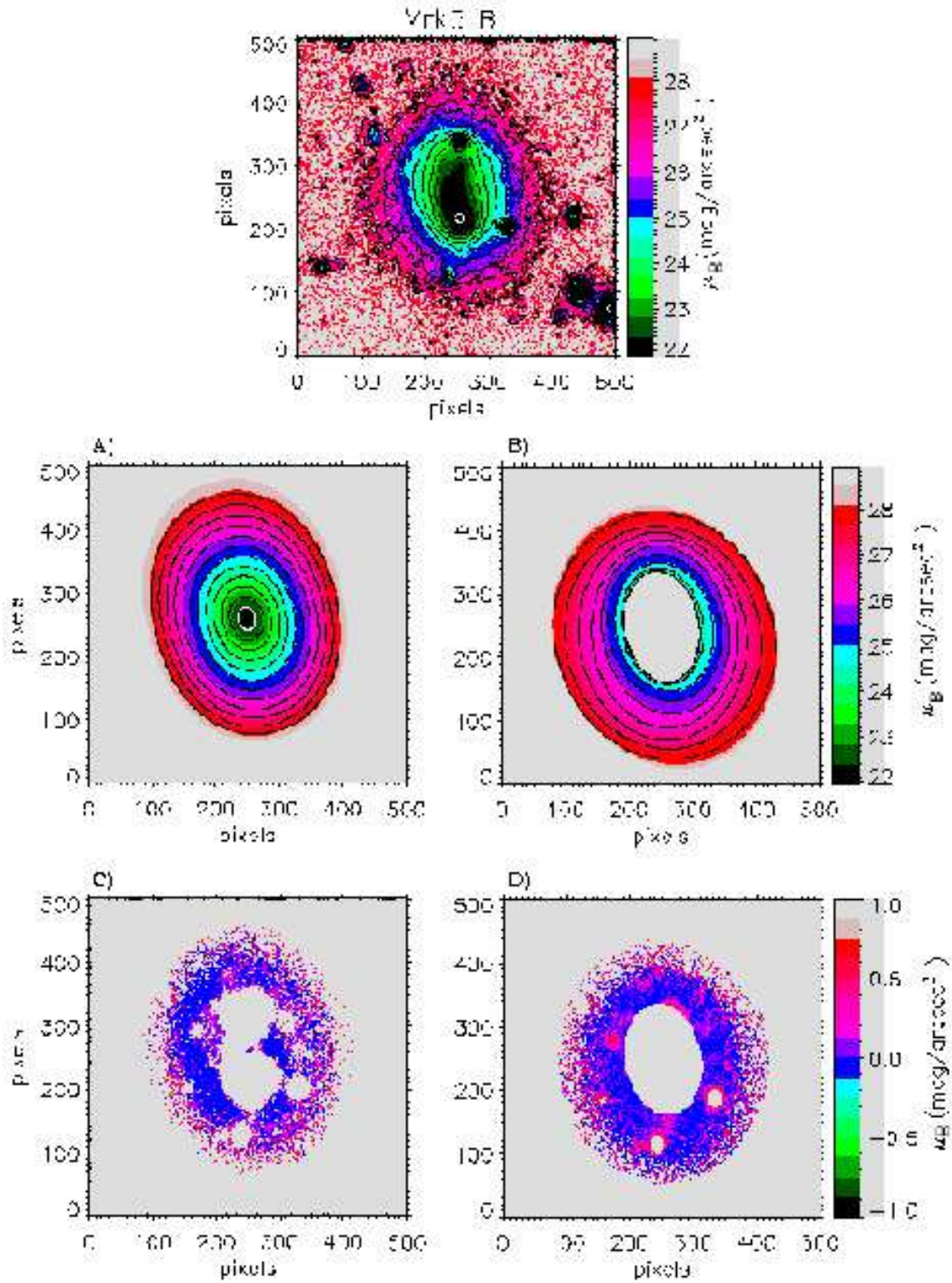


Fig. 13. Comparison between the GALFIT 2D model (panels A) and C) and the 2D model generated by using the *bmodel* task of IRAF from the 1D fit (Paper I) for Mrk 5 (panels B) and D)). In A) and B) we show the two models, while in C) and D) we show the residuals down to the $1\sigma_{sky}$ level.

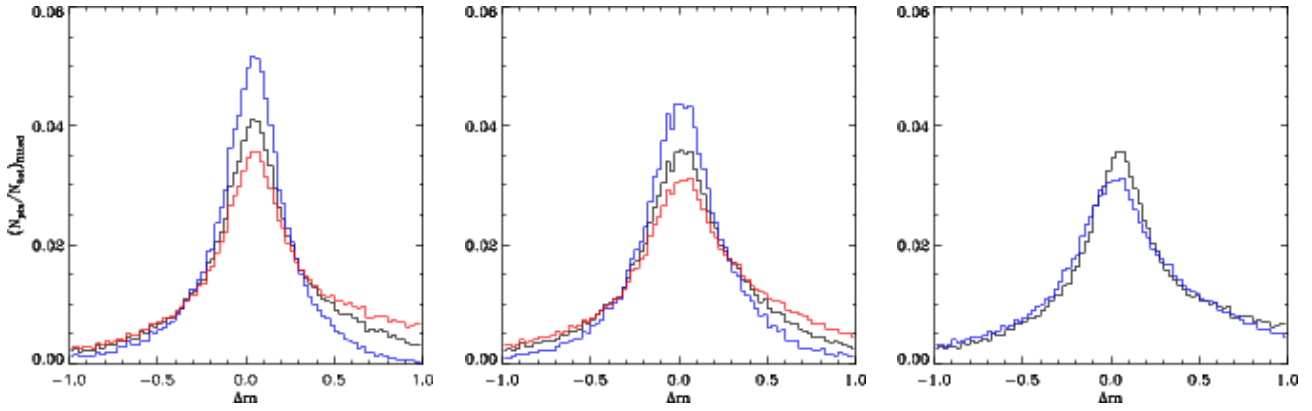


Fig. 14. Residual histograms for Mrk 5. Comparison between residuals provided from the 2D model and the 2D model generated from the 1D fit. See text in Section 4.3.1 for details.

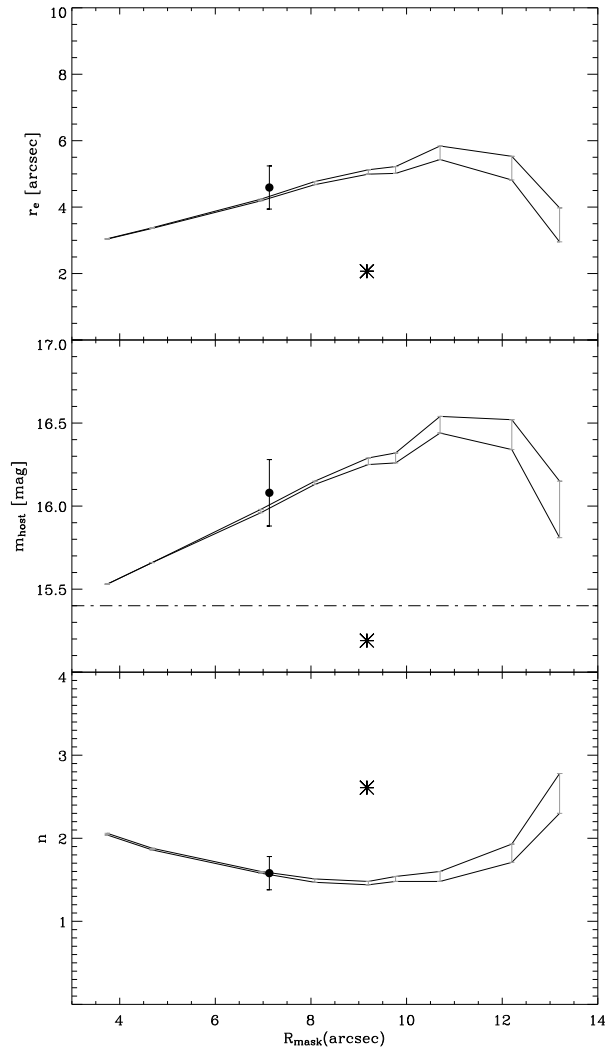


Fig. 15. I Zw 123 *B*-band: the free model parameters R_e , m_{tot} and n , are plotted as a function of R_{mask} . Dots are the final best 2D fits. Their R_{mask} value correspond to the radius beyond which starburst emission is practically absent, R_{tran} . Results from Paper I for each parameter are also indicated by asterisks. The horizontal dashed-dotted line in the m_{tot} plot indicates the magnitude of the whole galaxy (host + starburst).